This is a non-peer reviewed pre-print submitted to EarthArXiv.

This manuscript is undergoing peer review at *Nature Geoscience*.

13.01.2026

# Global sediment transport intermittency is set by river planform

Jonah S. McLeod[1,2]*, Vamsi Ganti[3,4], Gary J. Hampson[1], Rebecca E. Bell[1], Louise J. Slater[5], Yinxue Liu[5], Huck C. Rees[3], Alexander C. Whittaker[1].

[1] Department of Earth Science and Engineering, Imperial College London; SW7 2AZ, UK.

[2] Grantham Institute, Science and Solutions for a Changing Planet DTP; London SW7 2AZ, UK.

[3] Department of Geography, University of California Santa Barbara; California 93106, USA.

[4] Department of Earth Science, University of California Santa Barbara; California 93106, USA.

[5] School of Geography and the Environment, University of Oxford; Oxford, OX1 3QY, UK.

*jonah.mcleod18@imperial.ac.uk

## Abstract

Patterns of water and sediment flux in rivers are key to understanding landscape responses to environmental change. Quantifying water intermittency in rivers (from perennial to ephemeral) provides vital context for interpreting long-term hydrographs and flood frequency, yet controls on corresponding sediment intermittency are poorly understood due to measurement challenges. We present the first global dataset quantifying both water and sediment intermittency in >300 river reaches across all climate zones. Results reveal water and sediment intermittency are decoupled worldwide: sediment intermittency is primarily controlled by river planform ($R^2$=0.47, $p<10^{-3}$), the plan-view morphology of rivers encompassing sinuosity and channel-count, while water intermittency is set by climate. We provide a mechanistic framework explaining the global variability in water and sediment intermittency, demonstrating that river planforms buffer climate-driven discharge variation and dampen these signals in sedimentary deposits. Our results permit stronger constraints on the impacts of intensifying hydrological variability in the near future, and the timescales of river activity across the solar system.

## Introduction

Rivers shape our planet, supporting life by conveying water and sediment from uplands to oceans. Understanding variability in river sediment and water transport through time is crucial for managing flood risk for >3 billion people living on large-river corridors (*1*) and for reconstructing past environments on Earth and Mars (*2–5*). However, the controls on this variability remain poorly understood, especially the mechanisms that cause river-to-river differences in sediment and water transport worldwide. This knowledge gap hinders our ability to predict how rivers may respond to climate and land-use changes, which globally alter water and sediment supplies (*1*, *6–8*).

For alluvial rivers—those with mobile bed and bank materials—river activity can be characterized using an intermittency factor, *I*, representing the ratio of a river's long-term average water or sediment discharge to its bankfull water or sediment discharge capacity (*9–12*). Bankfull water discharge is the highest flow that a river can carry before it floods (breaches its banks), often considered to approximate the discharge that maximizes sediment export over geologic timescales (*13–15*). Theoretically, when a river has a high intermittency factor (approaching 1), it indicates near-perennial transport of water or sediment at or near channel capacity (Fig. 1A-C). Lower values (approaching 0) reveal that rivers concentrate much of their transport in infrequent, extreme events (Fig. 1D-F). This intermittency determines the sediment-export timescales that regulate the global carbon cycle (*16–18*), governs how environmental signals are transmitted into the sedimentary record (*19*, *20*) and is the key unknown in constraining past timescales of fluvial activity on Earth and other planetary bodies (*3*, *4*).

Intermittency factors for sediment and water are routinely assumed in hydrological and landscape-evolution models (*3*), yet these assumptions often have large uncertainties (*4*, *21*). Previous work suggests that sediment and water intermittency can vary with climate-driven weather patterns (*3*, *9*), channel geometry (*22*) and catchment length and slope (*23*). Additionally, a regional-scale study revealed a correlation between sediment intermittency and the relative sediment-to-water supply (*3*). However, we lack global-scale assessments of water and sediment intermittency due to historical limitations in quantifying both instantaneous and long-term water and sediment discharge rates in rivers worldwide, and in estimating the bankfull transport capacities of rivers.

Recent advances now facilitate a global assessment of river intermittency. Extensive new observational water discharge compilations allow estimation of bankfull water discharge at scale (*24*), and new field measurements permit calculation of sediment flux rates (*9*). Furthermore, increasing coverage of high-resolution satellite imagery also enables quantitative measures of river planform, the plan-view morphology of rivers (e.g., single- or multi-threaded (*25*)). River planform is an emergent phenomenon that arises due to the competition between bank erosion rates and lateral accretion rates of the opposite bank (*26*), and is a complex function of geomorphic bounding conditions such as channel slope, sediment supply, grain-size distribution, bank cohesion and vegetation. Here we employ these tools to

build a dataset of water and sediment intermittency for up to 513 1 km-long reaches across seven continents, including meandering, wandering and braided rivers. We show that water and sediment transport intermittency are decoupled: climate governs water intermittency, while river planform, not climate, exerts a primary control on sediment intermittency.

## A global view of river intermittency

We established a global view of water ($I_w$) and sediment ($I_s$) intermittency by integrating long-term observational water discharge data (*27*), global-scale sediment transport models (*28*), sediment flux theory (*29–31*), and a recently published global dataset estimating bankfull water discharge (*24*) (see SI for extended methodology). We compiled our database of alluvial river reaches from a global survey (*27*) ($N$ = 297) incorporating measurements of river planform shape, river bed slope, and water discharge; a regional database of sediment intermittency from the contiguous USA and Antarctica (*3*) ($N$ = 200); and field measurements in Greece (*9*) ($N$ = 16). Together, our data describe 513 reaches (Fig. 1I) of 1 km in length, spanning all continents and climate zones. These rivers range in width from 3 m to 7 km, have riverbed slopes between $2.0\text{x}10^{-5}$ and $1.2\text{x}10^{-1}$, drain upstream catchment areas of $5.2\text{x}10^{-1}$ km$^2$ to $2.9\text{x}10^{6}$ km$^2$, and encompass all river planform shapes: braided, wandering and meandering (*25*, *27*, *32*).

For each reach in our dataset, we estimated water and sediment intermittency as the ratio between the average and the bankfull water or sediment flux. This ratio represents a theoretical or linearized fraction of time required to transport the average water or sediment load if the river flowed continuously at bankfull capacity (*10*). We quantified $I_w$ by normalizing the long-term discharge mean (based on observational records) by the estimated bankfull water discharge (*11,* SI). To calculate $I_s$, we used a sediment discharge model (*28*, *33*) to estimate the long-term bed material transport rates due to the sparsity of sediment discharge gauges. We calculated bankfull sediment transport capacity using well-established theory (*29*, *30*), following previous work (*3*, *5*, *9*). We quantified channel planform using the Channel Form Index (*CFI*) (*27*), an adaptation which allows for both the categorization of river morphologies and their analysis using a continuous metric based on measures of river sinuosity and channel count which were derived from satellite imagery. In this parameter space, meandering rivers generally have $CFI > 1.0$, braided rivers have $CFI < 0.4$, and the intermediate values indicate wandering rivers. In addition, we categorized each reach using the four classified Köppen-Geiger climate zones (Tropical, Temperate, Arid, and Cold & Polar) (*34*, *35*). Our analysis yielded $I_s$ values and climate zones for all 513 reaches; however, limitations in remote sensing of small rivers restrict *CFI* estimates to 316 reaches, and $I_w$ data are limited to 297 reaches due to the scarcity of gauged rivers worldwide (Fig 1I).

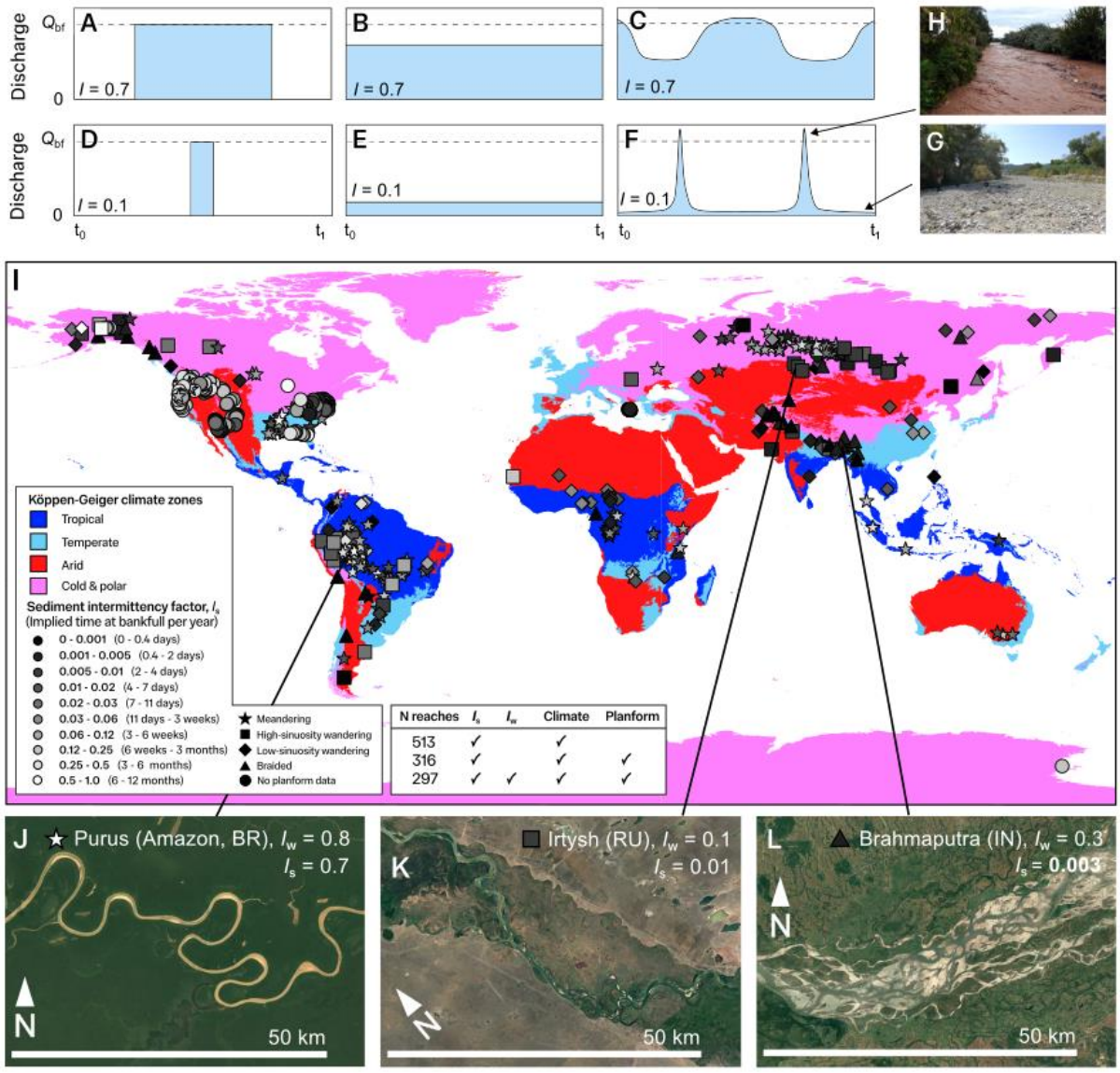


**Figure 1.** Summary of river intermittency and the global intermittency dataset. (A-C) Schematic hydrographs for a river with an intermittency factor (*I*) of 0.7; $t_0$-$t_1$ denotes an arbitrary time-step (e.g., 1 year). Sediment intermittency factors represent the ratio of average to bankfull sediment transport rates, and water intermittency refers to the ratio of average to bankfull water discharge rates. The area under the hydrograph can be distributed in many ways (*11*), and could represent a water or sediment hydrograph. (D-F) As above, but for *I*=0.1. (G-H) Photographs of ephemeral rivers in Greece at bankfull discharge (G) and during low or no flow (H). Field data from this river are included in our study. (I) Global map of our intermittency dataset: continents are coloured by Köppen-Geiger climate zone (*34*, *35*), with river reach markers shaded by sediment intermittency factor and shaped by planform. The summary box indicates dataset size for four key parameters. (J-L) Example rivers illustrating variability in water intermittency and planform: (J) a meandering reach of the Purus River, Amazon basin, Brazil; (K) a high-sinuosity wandering reach of the Irtysh River, Russia; and (L) a braided reach of the Brahmaputra River, India.

Results reveal that water intermittency factor ($I_w$) varies from $6.2 \times 10^{-3}$ to ca. 1.0 across the 297 reaches (Fig. 1I), with a mean and median of 0.31 and 0.25, respectively. These intermittency factors can be conceptualized (as in Fig. 1A) as the fraction of time of bankfull discharge required to meet long-term average rates. Considering a hypothetical 1-year hydrograph, these global $I_w$ values averaging 0.25-0.31 suggest that most rivers could theoretically complete their annual water budget in 3-4 months (c. 25-30% of 1 year) of sustained bankfull flow. Notably, $I_w$ varied with climate. We found that average $I_w$ in tropical and temperate zones was similar, with 25$^{th}$ and 75$^{th}$ percentiles ranging from 0.24 to 0.50 and 0.16 to 0.42, respectively (Fig. 2A). However, Kruskal–Wallis H-tests revealed significantly lower median $I_w$ values in arid and cold climate zones (p-value < $10^{-3}$) with 25$^{th}$ and 75$^{th}$ percentiles ranging from 0.13 to 0.31, and 0.13 to 0.25, respectively. These lower $I_w$ values (Fig. 2A) imply patterns of river flow that, if concentrated into a sustained bankfull event, could complete annual water budgets with only ca. 6 weeks of bankfull flow, suggesting flashier discharge regimes. Our global dataset demonstrates that hydroclimate is the primary determinant of water intermittency.

In contrast, $I_s$ remains relatively stable across climate zones (p = 0.4 for Kruskal-Wallis H-test), with median values of 0.04 and 0.03 for tropical and temperate reaches, and 0.02 and 0.03 for arid and cold reaches (Fig. 2A). This supports regional findings for rivers in the USA, where $I_s$ does not vary with aridity (*3*).

Our compilation enables direct comparison of $I_s$ and $I_w$ worldwide. For nearly all reaches (~98%), $I_s < I_w$, consistent with sediment transport being a threshold process requiring bed shear stresses to exceed a critical value to initiate sediment motion (*14*). The $I_s$ values span two orders of magnitude more than $I_w$ (Fig. 2B): $I_s$ ranges from $3.8 \times 10^{-5}$ to $9.9 \times 10^{-1}$, with mean and median values of $1.2 \times 10^{-1}$ and $3.3 \times 10^{-2}$, respectively (25$^{th}$ and 75$^{th}$ percentiles of $7.6 \times 10^{-3}$ to $1.5 \times 10^{-1}$), implying 1-13 weeks of bankfull sediment transport would equal the annual sediment budget. Notably, for a given $I_w$ value, $I_s$ can vary by more than four orders of magnitude (Fig. 2B), revealing that river water intermittency and sediment transport intermittency are decoupled and independent (t-test p<$10^{-3}$).

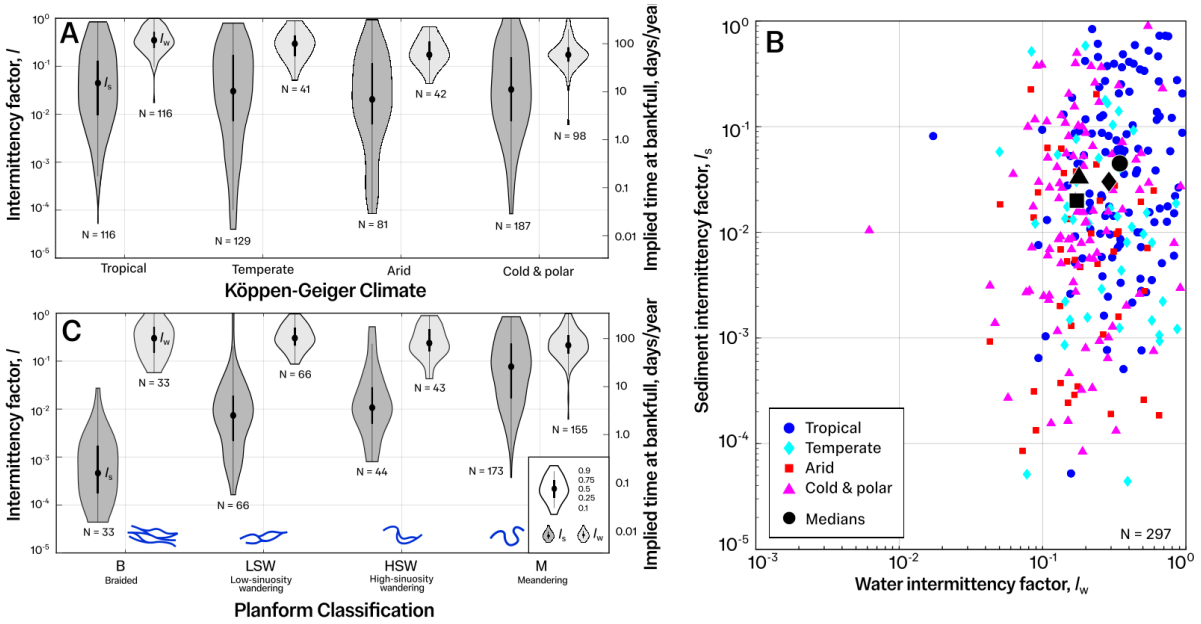


**Figure 2.** Intermittency results. (A) Violin plots illustrating the distribution of *I* by climate zone including the sediment intermittency factor, $I_s$ (dark grey), and the water intermittency factor, $I_w$ (light grey). $I_w$ varies with climate zone more than $I_s$. (B) Scatter plot of $I_s$ versus $I_w$, illustrating that $I_w$ and $I_s$ are decoupled globally. (C) Violin plots illustrating the distribution of $I_s$ and $I_w$ by river planform classification. Water intermittency is unrelated to planform, while sediment intermittency differs markedly between braided and meandering rivers, with wandering rivers showing intermediate $I_s$.

**Planform sets sediment intermittency**

Given that sediment intermittency is decoupled from water intermittency, we explored controls on $I_s$ variation worldwide. Rivers partition water and sediment into one or more channels, or threads, suggesting that planform style could affect transport patterns (*14*). Therefore, we segmented data into four major planform types (*27*) (Fig. 2C). Our analysis revealed a strong relationship between sediment intermittency and river planform. Braided rivers have the lowest $I_s$ values, with a median of $4.6 \times 10^{-4}$, implying that only 4-5 hours of sediment transport at bankfull rates can complete annual sediment budgets. Such low $I_s$ values suggest highly intermittent sediment transport dominated by a few extreme sediment-transport events (*9*). In contrast, meandering rivers were two orders of magnitude less intermittent, with a median $I_s$ value of $7.7 \times 10^{-2}$. These rivers could achieve their yearly sediment budget if bankfull transport were to be sustained for approximately 1 month. Kruskal–Wallis H-tests confirmed significant differences in median $I_s$ values among braided, wandering and meandering rivers ($p < 10^{-3}$), demonstrating a statistically significant link between $I_s$ and river planform.

Our analyses also show that the planform-intermittency relationship extends beyond these categorized morphological classifications: we find *CFI* and $I_s$ covary according to a power-law trend described by a quadratic formula across all planform morphologies (Fig. 3). This means that halving the *CFI*

(reducing sinuosity or increasing channel-thread count) is associated with a fourfold reduction in $I_s$. This pattern holds across all climate zones (Fig 3); however, $I_w$ does not covary with *CFI* in a given climate zone. A second-order polynomial regression between *CFI* and $I_s$ is consistent with established scaling laws which suggest that for the same discharge, increasing the number of threads causes a reduction in bankfull bed shear stress, thus reducing $I_s$ (see further explanation in Supplementary Information, SI). Multivariate regressions (SI) confirm that planform is the strongest predictor of changes in $I_s$, exceeding influences from slope, grain-size, catchment area, channel aspect ratio, or any other measured parameter included in our dataset. These results demonstrate that sediment transport patterns are highly sensitive to changes in river sinuosity and thread count within and across different climate zones.

**Implications and conclusions**

We globally characterized river intermittency to investigate water and sediment transport patterns in rivers (Fig. 1). Our results show that, while climate sets water intermittency, river planform primarily controls sediment transport intermittency: multi-thread rivers exhibit significantly lower sediment intermittency factors than single-thread rivers (Fig. 2). This global perspective reshapes our understanding of river activity, providing the most robust constraints to-date on the range and distribution of water and sediment intermittency across all climate zones and planform types. These results also provide a new mechanistic basis, outlined below (and discussed in SI), for the correlation between $I_s$ and relative sediment-to-water supply (*3*), which is widely considered an explanatory variable for river planform (*32*, *36*).

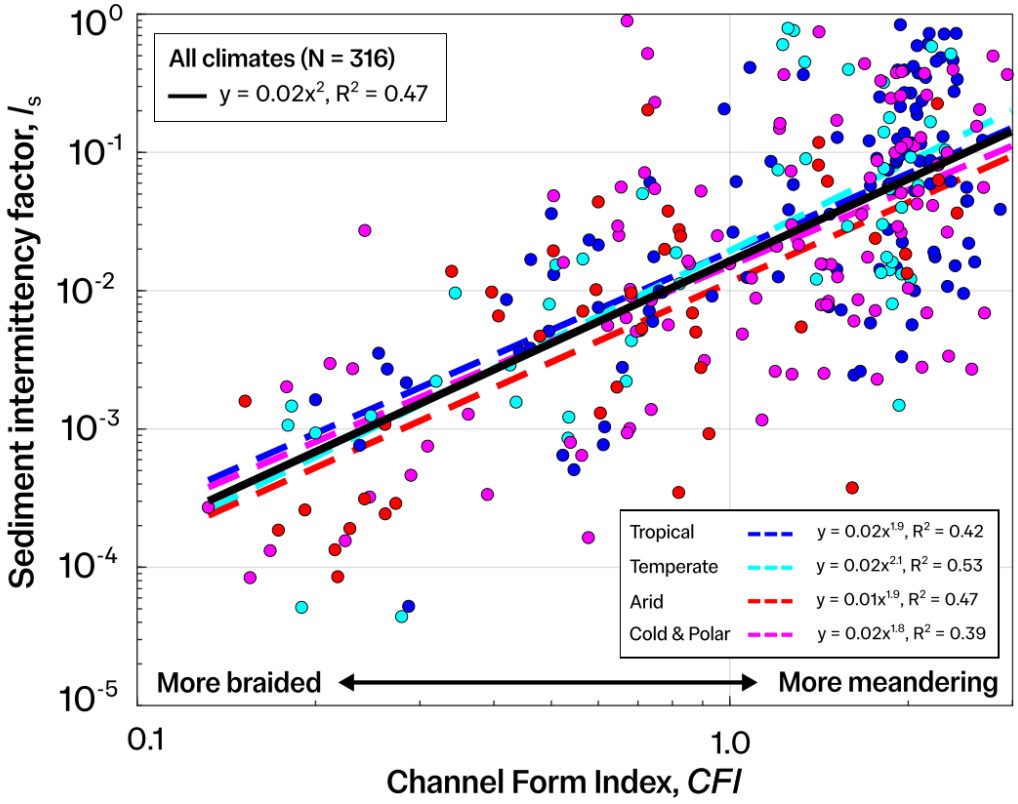


**Figure 3.** Global regression between sediment intermittency factor, $I_s$, and the Channel Form Index, *CFI*. $I_s$ increases with *CFI* (more meandering planform style is associated with more perennial river sediment transport) with an $R^2$ value of 0.47 and RMSE=0.18. This trend is independent of climate zone, demonstrating the continuous influence of river planform on sediment transport patterns.

Sediment intermittency factors are crucial for estimating the lifespan of ancient rivers on Earth and other planetary bodies (*3*, *4*, *9*). For example, rover and orbital imagery are increasingly facilitating investigations of Mars' ancient aridification, but intermittency factors are often assumed in these calculations (*3*), with wide uncertainty margins (*21*, *37*). Our dataset provides a benchmark for these intermittency factors, which are vital to upscale water or sediment volume estimates to durations or patterns of water and sediment discharge. For instance, previous work on meandering river deposits in Jezero Crater estimated $I_s$ values of ca. $10^{-4}$ (*4*); our work suggests that these values may be at least two orders of magnitude lower than typical values observed on Earth for similar deposits (*4*), even in cold and polar climates. Higher $I_s$ values may in turn suggest significantly shorter timescales for sustained fluvial activity than previously interpreted (*2*, *4*). Thus, the quantitative constraints on intermittency presented here can help refine the interpreted history of climate change across the solar system.

In addition to providing global estimates of intermittency, we demonstrate that water and sediment intermittency factors are decoupled worldwide (Fig. 2). Since sediment entrainment depends on bed shear stress, substantial sediment transport occurs when grain-size-specific entrainment thresholds are exceeded—conditions that arise only during certain discharge events (*14*). Consequently, sediment

intermittency is governed not only by water discharge but by river morphology, which modifies the frequency of sediment mobilization. We hypothesize that the observed $I_s$-$I_w$ decoupling arises from differences between the self-formed bankfull geometry of single- and multi-thread rivers (*38*, *39*), which can lead to differences in sediment mobilization. In single-thread rivers, bed shear stress at bankfull conditions coincides with the onset of substantial suspended sediment transport, whereas in multi-thread rivers it aligns with the threshold for motion of median bed material (*14*). Therefore, fluctuations in water discharge around the bankfull stage in multi-thread rivers can shift conditions from no bedload motion to significant bedload transport. Comparable discharge variations in single-thread rivers instead modify the concentration of suspended sediment, with sediment potentially being transported perennially even at conditions below bankfull discharge (*40*). Consequently, while sediment and water transport might intuitively be expected to covary, the observed differences in $I_s$ between braided and meandering rivers can be mechanistically linked to fundamental differences in sediment transport thresholds at bankfull conditions. This decoupling could also provide a new mechanism by which hydroclimatic signals are transformed into the sedimentary record (*19*), with long-term hydroclimatic variability likely buffered in sediment export and fluvial deposits (*14*).

Our finding that planform is the primary determinant of sediment intermittency has important implications for the evolution of Earth's landscapes under ongoing climatic and anthropogenic change (*1*, *6–9*). Multi-thread rivers with low $I_s$ values are especially susceptible to the magnitudes of discharge extremes because low $I_s$ rivers may often meet their annual sediment budgets in a single storm event (*9*, *41*). In many regions the magnitudes of storms are increasing while average precipitation rates are decreasing as a consequence of global warming (*42–44*), indicating that multi-thread rivers across the globe might be more susceptible to these changes in extremes. These effects may become even more pronounced in the near future given that human activities are further reshaping planform dynamics. Deforestation in tropical regions (e.g., Brazil (*45*), Colombia (*46*), Ecuador (*47*), Malaysia (*48*)), driven by demand for pastureland and lumber (*49–51*) is promoting accelerated bank migration, enhanced sediment loads and reduced bank stability, increasing the propensity for multi-thread planforms and consequently reduced $I_s$ values. This reduction in sediment intermittency can enhance the sensitivity of these systems to climate extremes, extend sediment export timescales, and consequently disrupt the carbon and nutrient cycle. In contrast to these regions, urban expansion is driving a proliferation of river channelisation and damming to regulate flood risk, and in many cases converting multi-thread rivers into single-thread morphologies (*52*, *53*). Our results suggest these forced planform changes may increase $I_s$, and in turn reduce sediment residence timescales with potential for long-lasting geomorphic consequences. Our dataset constrains how planform and discharge extremes interact to set sediment export timescales. Our results offer a framework to estimate timescales of fluvial activity on Mars, and to anticipate geomorphic impacts of intensifying hydrological variability, including evolving monsoon

cycles, sediment-driven flood hazards and damages to infrastructure, which are affecting billions of people worldwide.

**References**


1. J. Best, Anthropogenic stresses on the world's big rivers. *Nature Geosci* **12**, 7–21 (2019).

2. P. B. Buhler, C. I. Fassett, J. W. Head, M. P. Lamb, Timescales of fluvial activity and intermittency in Milna Crater, Mars. *Icarus* **241**, 130–147 (2014).

3. A. T. Hayden, M. P. Lamb, B. J. McElroy, Constraining the Timespan of Fluvial Activity From the Intermittency of Sediment Transport on Earth and Mars. *Geophysical Research Letters* **48** (2021).

4. M. Lapôtre, A. Ielpi, The Pace of Fluvial Meanders on Mars and Implications for the Western Delta Deposits of Jezero Crater. *AGU Advances* **1** (2020).

5. S. J. Lyster, A. C. Whittaker, A. Farnsworth, G. J. Hampson, Constraining flow and sediment transport intermittency in the geological past. *GSA Bulletin* **136**, 2425–2442 (2023).

6. D. Li, X. Lu, I. Overeem, D. E. Walling, J. Syvitski, A. J. Kettner, B. Bookhagen, Y. Zhou, T. Zhang, Exceptional increases in fluvial sediment fluxes in a warmer and wetter High Mountain Asia. *Science* **374**, 599–603 (2021).

7. IPCC, "IPCC, 2022: Climate Change 2022: Impacts, Adaptation, and Vulnerability. Contribution of Working Group II to the Sixth Assessment Report of the Intergovernmental Panel on Climate Change" (Cambridge University Press, Cambridge, UK and New York, NY, USA, 2022); https://www.ipcc.ch/report/ar6/wg3/.

8. E. N. Dethier, C. E. Renshaw, F. J. Magilligan, Rapid changes to global river suspended sediment flux by humans. *Science* **376**, 1447–1452 (2022).

9. J. S. McLeod, A. C. Whittaker, R. E. Bell, G. J. Hampson, S. E. Watkins, S. A. S. Brooke, N. Rezwan, J. Hook, J. R. Zondervan, V. Ganti, S. J. Lyster, Landscapes on the edge: River intermittency in a warming world. *Geology* **52**, 512–516 (2024).

10. C. Paola, P. L. Heller, C. L. Angevine, The large-scale dynamics of grain-size variation in alluvial basins, 1: Theory. *Basin Research* **4**, 73–90 (1992).

11. S. J. Lyster, A. C. Whittaker, A. Farnsworth, G. J. Hampson, Constraining flow and sediment transport intermittency in the geological past. *GSA Bulletin* **136**, 2425–2442 (2023).

12. J. A. Czuba, E. Foufoula-Georgiou, A network-based framework for identifying potential synchronizations and amplifications of sediment delivery in river basins. *Water Resources Research* **50**, 3826–3851 (2014).

13. M. G. Wolman, J. P. Miller, Magnitude and Frequency of Forces in Geomorphic Processes. *The Journal of Geology* **68**, 54–74 (1960).

14. C. B. Phillips, D. J. Jerolmack, Self-organization of river channels as a critical filter on climate signals. *Science* **352**, 694–697 (2016).

15. C. B. Phillips, C. C. Masteller, L. J. Slater, K. B. J. Dunne, S. Francalanci, S. Lanzoni, D. J. Merritts, E. Lajeunesse, D. J. Jerolmack, Threshold constraints on the size, shape and stability of alluvial rivers. *Nat Rev Earth Environ* **3**, 406–419 (2022).

16. M. A. Torres, A. B. Limaye, V. Ganti, M. P. Lamb, A. J. West, W. W. Fischer, Model predictions of long-lived storage of organic carbon in river deposits. *Earth Surface Dynamics* **5**, 711–730 (2017).

17. M. Repasch, J. S. Scheingross, N. Hovius, M. Lupker, H. Wittmann, N. Haghipour, D. R. Gröcke, O. Orfeo, T. I. Eglinton, D. Sachse, Fluvial organic carbon cycling regulated by sediment transit time and mineral protection. *Nat. Geosci.* **14**, 842–848 (2021).

18. E. C. Geyman, Y. Ke, J. S. Magyar, J. N. Reahl, V. Soldano, N. D. Brown, A. J. West, W. W. Fischer, M. P. Lamb, Scaling laws for sediment storage and turnover in river floodplains. *Science Advances* **11**, eadu8574 (2025).

19. D. J. Jerolmack, C. Paola, Shredding of environmental signals by sediment transport. *Geophysical Research Letters* **37** (2010).

20. K. M. Straub, R. A. Duller, B. Z. Foreman, E. A. Hajek, Buffered, Incomplete, and Shredded: The Challenges of Reading an Imperfect Stratigraphic Record. *Journal of Geophysical Research: Earth Surface* **125**, e2019JF005079 (2020).

21. E. Hauber, K. Gwinner, M. Kleinhans, D. Reiss, G. Di Achille, G.-G. Ori, F. Scholten, L. Marinangeli, R. Jaumann, G. Neukum, Sedimentary deposits in Xanthe Terra: Implications for the ancient climate on Mars. *Planetary and Space Science* **57**, 944–957 (2009).

22. C. B. Phillips, D. J. Jerolmack, Bankfull Transport Capacity and the Threshold of Motion in Coarse-Grained Rivers. *Water Resour. Res.* **55**, 11316–11330 (2019).

23. P. A. Allen, J. J. Armitage, A. Carter, R. A. Duller, N. A. Michael, H. D. Sinclair, A. L. Whitchurch, A. C. Whittaker, The Qs problem: Sediment volumetric balance of proximal foreland basin systems. *Sedimentology* **60**, 102–130 (2013).

24. Y. Liu, M. Wortmann, L. Hawker, J. Neal, J. Yin, M. S. Santos, B. Anderson, R. Boothroyd, A. Nicholas, G. S. Smith, P. Ashworth, H. Cloke, S. Gebrechorkos, J. Leyland, B. Zhang, E. Vahidi, H. Griffith, P. Delorme, S. McLelland, D. Parsons, S. Darby, L. Slater, Global Estimation of River Bankfull Discharge Reveals Distinct Flood Recurrences Across Different Climate Zones. In Review [Preprint] (2024). https://doi.org/10.21203/rs.3.rs-5185659/v1.

25. L. B. Leopold, M. G. Wolman, "River channel patterns: Braided, meandering, and straight" (282-B, U.S. Government Printing Office, 1957); https://doi.org/10.3133/pp282B.

26. A. J. Chadwick, E. Greenberg, V. Ganti, Single- and multithread rivers originate from (im)balance between lateral erosion and accretion. *Science* **389**, 146–150 (2025).

27. C. P. Galeazzi, R. P. Almeida, A. H. do Prado, Linking rivers to the rock record: Channel patterns and paleocurrent circular variance. *Geology* **49**, 1402–1407 (2021).

28. S. Cohen, A. J. Kettner, J. P. M. Syvitski, B. M. Fekete, WBMsed, a distributed global-scale riverine sediment flux model: Model description and validation. *Computers & Geosciences* **53**, 80–93 (2013).

29. F. Engelund, E. Hansen, A monograph on sediment transport in alluvial streams. *Technical University of Denmark 0stervoldgade 10, Copenhagen K.* (1967).

30. E. Meyer-Peter, R. Müller, Formulas for Bed-Load transport. *IAHSR 2nd meeting, Stockholm, appendix 2* (1948).

31. M. Wong, G. Parker, Reanalysis and Correction of Bed-Load Relation of Meyer-Peter and Müller Using Their Own Database. *J. Hydraul. Eng.* **132**, 1159–1168 (2006).

32. L. B. Leopold, T. Maddock, *The Hydraulic Geometry of Stream Channels and Some Physiographic Implications* (U.S. Government Printing Office, 1953).

33. S. Cohen, J. Syvitski, T. Ashley, R. Lammers, B. Fekete, H.-Y. Li, Spatial Trends and Drivers of Bedload and Suspended Sediment Fluxes in Global Rivers. *Water Resources Research* **58**, e2021WR031583 (2022).

34. W. Köppen, Die Wärmezonen der Erde, nach der Dauer der heissen, gemässigten und kalten Zeit und nach der Wirkung der Wärme auf die organische Welt betrachtet. *Meteorologische Zeitschrift* **1**, 215–226 (1884).

35. H. E. Beck, N. E. Zimmermann, T. R. McVicar, N. Vergopolan, A. Berg, E. F. Wood, Present and future Köppen-Geiger climate classification maps at 1-km resolution. *Sci Data* **5**, 180214 (2018).

36. M. Kleinhans, J. H. Berg, River channel and bar patterns explained and predicted by an empirical and physics-based method. *Earth Surface Processes and Landforms* **36**, 721–738 (2011).

37. M. G. A. Lapôtre, A. Ielpi, The Pace of Fluvial Meanders on Mars and Implications for the Western Delta Deposits of Jezero Crater. *AGU Advances* **1**, e2019AV000141 (2020).

38. G. Parker, On the cause and characteristic scales of meandering and braiding in rivers. *Journal of Fluid Mechanics* **76**, 457–480 (1976).

39. K. B. J. Dunne, D. J. Jerolmack, Evidence of, and a proposed explanation for, bimodal transport states in alluvial rivers. *Earth Surface Dynamics* **6**, 583–594 (2018).

40. E. Viparelli, J. A. Nittrouer, G. Parker, Modeling flow and sediment transport dynamics in the lowermost Mississippi River, Louisiana, USA, with an upstream alluvial-bedrock transition and a downstream bedrock-alluvial transition: Implications for land building using engineered diversions. *Journal of Geophysical Research: Earth Surface* **120**, 534–563 (2015).

41. B. W. Romans, S. Castelltort, J. A. Covault, A. Fildani, J. P. Walsh, Environmental signal propagation in sedimentary systems across timescales. *Earth-Science Reviews* **153**, 7–29 (2016).

42. K. Goubanova, L. Li, Extremes in temperature and precipitation around the Mediterranean basin in an ensemble of future climate scenario simulations. *Global and Planetary Change - GLOBAL PLANET CHANGE* **57**, 27–42 (2007).

43. S. Westra, H. J. Fowler, J. P. Evans, L. V. Alexander, P. Berg, F. Johnson, E. J. Kendon, G. Lenderink, N. M. Roberts, Future changes to the intensity and frequency of short-duration extreme rainfall: FUTURE INTENSITY OF SUB-DAILY RAINFALL. *Rev. Geophys.* **52**, 522–555 (2014).

44. Y. Tramblay, S. Somot, Future evolution of extreme precipitation in the Mediterranean. *Climatic Change* **151**, 289–302 (2018).

45. E. M. Latrubesse, M. L. Amsler, R. P. de Morais, S. Aquino, The geomorphologic response of a large pristine alluvial river to tremendous deforestation in the South American tropics: The case of the Araguaia River. *Geomorphology* **113**, 239–252 (2009).

46. J. D. Restrepo, A. J. Kettner, J. P. M. Syvitski, Recent deforestation causes rapid increase in river sediment load in the Colombian Andes. *Anthropocene* **10**, 13–28 (2015).

47. V. Vanacker, A. Molina, G. Govers, J. Poesen, G. Dercon, S. Deckers, River channel response to short-term human-induced change in landscape connectivity in Andean ecosystems. *Geomorphology* **72**, 340–353 (2005).

48. A. J. Horton, J. A. Constantine, T. C. Hales, B. Goossens, M. W. Bruford, E. D. Lazarus, Modification of river meandering by tropical deforestation. *Geology* **45**, 511–514 (2017).

49. H. Ritchie, M. Roser, Land Use. *Our World in Data* (2019).

50. J. Poore, T. Nemecek, Reducing food's environmental impacts through producers and consumers. *Science* **360**, 987–992 (2018).

51. E. Stehfest, L. Bouwman, D. P. van Vuuren, M. G. J. den Elzen, B. Eickhout, P. Kabat, Climate benefits of changing diet. *Climatic Change* **95**, 83–102 (2009).

52. S. Hohensinner, B. Lager, C. Sonnlechner, G. Haidvogl, S. Gierlinger, M. Schmid, F. Krausmann, V. Winiwarter, Changes in water and land: the reconstructed Viennese riverscape from 1500 to the present. *Water Hist* **5**, 145–172 (2013).

53. V. Scorpio, F. Comiti, F. Liébault, H. Piegay, M. Rinaldi, N. Surian, Channel changes over the last 200 years: A meta data analysis on European rivers. *Earth Surface Processes and Landforms* **49**, 2651–2676 (2024).

**Funding:**

Natural Environment Research Council grant NE/S007415/1 (JSM)

Terrabotics London (JSM)

**Author contributions:**

Conceptualization: JSM, VG

Methodology: JSM, VG, ACW, HCR, LJS, YL

Investigation: JSM, VG, ACW

Visualization: JSM, VG, ACW

Project administration: JSM, ACW, VG

Supervision: ACW, GJH, REB, VG

Writing – original draft: JSM

Writing – review and editing: JSM, VG, GJH, REB, LJS, YL, HCR, ACW

**Competing interests:**

The authors declare that they have no competing interests.

**Data and materials availability:**

All data used in analyses are available in the Supplementary Information

**Supplementary Information**

Supplementary Text

Figs. S1 to S5

Supplementary Data

This Supplementary Information is associated with a non-peer reviewed pre-print submitted to EarthArXiv.

The manuscript is undergoing peer review at *Nature Geoscience*.

13.01.2026

Supplementary Information for

# Global sediment transport intermittency is set by river planform

Jonah S. McLeod[1,2], Vamsi Ganti[3,4], Gary J. Hampson[1], Rebecca E. Bell[1], Louise J. Slater[5], Yinxue Liu[5], Huck Rees[3], Alexander C. Whittaker[1].

Corresponding author: jonah.mcleod18@imperial.ac.uk

## Contents

This PDF file includes:



**Other Supplementary Information for this manuscript include the following:**

Supplementary Data

## Introduction

This Supplementary Information contains extended methodology and discussion. First, we present detailed methodology for data collection, compilation and calculations, and associated sources of uncertainty. Second, we discuss the results of regression analyses and the mechanistic explanation for the observed trend between river planform and sediment intermittency factor.

## Materials and Methods

### Data compilation

In order to estimate intermittency factors for modern rivers, we need the long-term average and instantaneous bankfull fluxes of water ($Q_{w(avg)}$ and $Q_{w(bf)}$, respectively) or sediment ($Q_{s(avg)}$ and $Q_{s(bf)}$, respectively) for river reaches across the world.

For $Q_{w(avg)}$, we used a large observational discharge dataset (*1*), compiled from river gauges with a range of record durations, including the Global Runoff Data Centre, national water agencies, geological surveys, and published hydrological studies. For the $Q_{w(bf)}$, we used the Global Bankfull Discharge (GQBF) dataset (*2*). This dataset estimated $Q_{w(bf)}$ for rivers worldwide based on observational $Q_{w(bf)}$ data and 31 predictors of river characteristics and climate. The GQBF model was trained on 2,657 observational $Q_{w(bf)}$ sites and applied globally using 31 geomorphic and climatic predictors across the GRIT network, a global 30 m hydrography produced from FABDEM (Forest and Buildings Removed Copernicus Digital Elevation Model, or Digital Terrain Model) drainage density model, combined with the GRWL Landsat-derived river mask.

For some of our $I_s$ dataset, we used previously reported data from USA and Antarctica rivers (*3*). In order to expand and build on this dataset we estimated $Q_{s(avg)}$, the average total bed-material flux, for a further 348 river reaches using WBMsed (*4*, *5*), a model which simulates spatially and temporally explicit (pixel scale and daily) sediment fluxes across the continents. The WBMsed model is grounded in BQART, a global empirical model that calculates long-term suspended sediment loads, the Psi statistical model which accounts for intra- and interannual variability in these BQART sediment flux predictions, and WBMplus, a global daily water balance/transport model. WBMsed outputs have been tested on observed sediment loads, BQART predictions and daily sediment flux observations, and strongly predict observed values (see Section 2.3 for further discussion of uncertainty in this model).

Observational measurements of $Q_{s(bf)}$ are limited in modern rivers. To calculate $Q_{s(bf)}$ for 348 rivers we followed a similar approach to one which has been successfully applied to rivers in the USA (*3*), using empirical-theoretical sediment transport relations. We first estimated the median bed material grain-size, $D_{50}$, from WBMsed (*5*), which models sediment grade, and checked against measured values where available. We then used these sediment grain-size values to estimate the bankfull flow depth (*6*) (see detailed methods in Section 2.2). Subsequently, for sand-bedded rivers, we used the formula of Engelund & Hansen (*7*) and for gravel-bedded rivers we use an approach based on the Meyer-Peter & Muller (*8*, *9*) relation for bedload transport. These equations have been routinely used in numerous field settings to estimate the sediment transport capacity of rivers to good effect (see Section 2.3 for further detail on uncertainty). We also conducted this analysis for 16 rivers in the Gulf of Corinth, Greece.

We additionally quantified planform morphology for a further 19 reaches not included in the original compilation of Galeazzi (*1*). For these 19 reaches, we extracted channel length and CCI from the Global River Widths from Landsat (GRWL) database (*10*). We divided the reach channel length by the valley length to derive sinuosity, and divided the resulting sinuosity by CCI to evaluate CFI, as discussed in the main text. This results in a dataset which describes river morphology and transport dynamics across every climate zone on Earth.

<u>Calculating intermittency</u>

The intermittency factor can be formally defined as

$$I = \frac{\Sigma Q(t)}{Q_{bf}\Sigma t}, \text{ (Eq. 1)}$$

where $\Sigma Q(t)$ is the total flux of water or sediment over a time interval, and $Q_{bf}\Sigma t$ is the bankfull flux totalled across the time interval (*11*). To calculate water intermittency, we used 361 observational values

of long-term average water discharge . Short-term bankfull discharge estimates were then acquired from the GQBF dataset (*2*). We selected each 1 km reach in GQBF corresponding to the gauging station from which average water discharge was acquired. In some cases, the gauging station does not correspond to a river reach covered in GQBF, so we did not estimate intermittency factors for these reaches.

For sediment intermittency, we estimated long-term average sediment flux rates using WBMsed model (*4*, *5*). In QGIS, we extracted the bed material sediment flux and particle size outputs from WMBsed. We then compared this dataset to the river reaches covered in GQBF and water discharge gauging stations. We selected the highest pixel value within 3 pixels of the gauging station and extracted the particle size, bedload flux and suspended bed material load flux. The sum of the bedload flux and suspended bed material load flux was calculated to estimate the average total bed material flux ($Q_{s(avg)}$). To calculate bankfull sediment flux rates, we used the particle size outputs of WBMsed to the median grain-size, $D_{50}$. Where $D_{50}$>2mm, we applied a dimensional hydraulic geometry prediction (*6*) to estimate bankfull flow depth, $H$:

$$H = \alpha_h Q^{0.4+n_h} g^{-2-0.5n_h} D_{50}^{-2.5n_h}, \text{ (Eq. 2)}$$

where $Q$ is discharge and $\alpha_h$, $m_h$ and $n_h$ are constants. And where $D_{50}$<2mm we estimated $H$ using the formula (*6*):

$$H = \alpha_h Q^{0.4+n_h} g^{0.5(m_h-n_h)-0.2} D_{50}^{1.5m_h-2.5n_h} R^{0.5m_h} \nu^{-m_h}, \text{ (Eq. 3)}$$

where $R$ is the sediment-water density differential and $\nu$ is the kinematic viscosity. Having estimated bankfull flow depth, $H$, we then use well-established and widely used sediment transport relations to acquire estimates of sediment flux. The following empirical-theoretical scaling relations have been used effectively to estimate sediment transport capacities of rivers across the solar system, trained on extensive field data, and models strongly predict observations. For sand-bedded reaches we calculate sediment flux per unit width, $q_s$ (*7*) in units of $m^2/s$ as:

$$q_s = q_t^* \left(RgD_{50}^3\right)^{0.5} \text{ , (Eq. 4)}$$

where $R$ is the submerged density of sediment (~1.65 for quartz), $g$ is 9.81 $m/s^2$, and $q^*_t$ is the dimensionless Einstein number, given as

$$q_t^* = \frac{0.05}{C_f} (\tau_*)^{\frac{5}{2}} \text{ , (Eq. 5)}$$

for which

$$C_f^{-1/2} = \frac{1}{\kappa} \ln\left(\frac{11H_s}{k_s}\right) \sqrt{\frac{\tau_*}{\tau_{*s}}} \text{ . (Eq. 6)}$$

In Equation 6, $k_s$ is a grain roughness length scale, $\kappa$ is the Von Karman constant, 0.41, and $H_s$ and $T^*_s$ are components of flow depth and shields stress due to skin friction (*12*). The flow depth due to skin friction, $H_s$, is calculated as:

$$H_s = (\tau_{*s} R D_{50})/S \text{ , (Eq. 7)}$$

and the roughness parameter $k_s$ is based on the bed grainsize:

$$k_s = n_k D_{50} \text{ , (Eq. 8)}$$

where $n_k = 2.5$ (*12*). The skin friction component of the total Shields stress is related to the total Shields stress as (*7*):

$\tau_{*s} = 0.06 + 0.4\tau_*^2$ for $\tau_{*s} \leq \tau\_*$ (Eq. 9)

$\tau_{*s} = \tau_*$ for $\tau_{*s} > \tau_*$ (Eq. 10)

In which $\tau_* = HS/RD_{50}$ . (Eq. 12)

For gravel-bedded reaches, we calculated unit bedload sediment flux using the empirical-theoretical scaling relation (*8*, *9*):

$Q_{s,bf} = \left(g\, {D_{50}}^3\, \Delta\rho\right)^{0.5} C(\tau_{*b} - \tau_{*c})^{\alpha}$ , (Eq. 13)

where Δρ is the dimensionless submerged specific gravity of sediment (1.6); dimensionless basal shear stress $\tau^*_b$ is given as

$\tau_{*b} = H_{bf}S\,/\Delta\rho D_{50}$ , (Eq. 14)

(*30*)

and dimensionless critical shear stress $\tau_{*c}$ and constants *C* and α are taken as 0.047, 4.93 and 1.6, respectively (*9*).

Outliers

Since the intermittency factor is ratio between average and bankfull conditions, it is unlikely for intermittency factors to be greater than 1. Where $I > 1$ it suggests rivers that may be in flood for large portions of the year. In our analysis we did recover some intermittency factors greater than 1 for both water and sediment. We found 4% of the dataset had $I > 1$, but we observed no statistically significant pattern determining which reaches have $I > 1$. Generally, however, most of these reaches have low values of channel slope, indicating these outliers often represent distal fluvial activity. Whilst no correlation is observed between outliers and discharge, all reaches with $I_w > 1$ are found in major channels of the Yangtze, Zambezi, Ganges, Bramaputra, Mississippi, Cauca, and Orinoco in tropical and temperate climate zones. This indicates fluvial transport dominated by high discharge with potential for sustained bankfull conditions. An alternative explanation is that these outliers arise in our dataset due to uncertainty in the GQBF dataset or in measured or calculated discharge values, such as where discharge gauges may have over-estimated mean flow rates. Consequently, we did not include this 4% of our dataset from our analyses, since they could represent anomalous values of $Q_m$ or $Q_{bf}$, or that some WBMsed and grain-size predictors are anomalous. The remainder of the dataset (ca. 96% where $I < 1$) reflect the notion that the majority of Earth's rivers have average discharges that are substantially lower than bankfull capacities.

Uncertainty

Our analysis is based on primary collected field data, model outputs and data collated from published datasets. There are, accordingly therefore, some sources of potential uncertainty. The average water discharge rates are the most robust in our dataset contributing to $I_w$ values, as these are a direct estimate from observational data (*1*). Whilst instrumental factors may introduce some uncertainty into these values, the $Q_{w(avg)}$ rates calculated lie within expected ranges. Our values of $Q_{w(bf)}$ are extracted from the global GQBF estimated dataset (*2*). The core observational dataset on which GQBF is based contains 194 reaches. The estimated dataset strongly predicts observed values, with $R^2$=0.72. The core

observational dataset is concentrated mostly in North and South America. While the key trend in our results, that between $I_s$ and *CFI*, is observed across all climates, there is some difference in error between different climate groups. In tropical rivers, $I_s$ and *CFI* regress with an $R^2$ value of 0.42 and a root mean squared error (RMSE) of 0.19. Temperate rivers have $R^2$=0.53 and RMSE=0.21, arid rivers have $R^2$=0.47 and RMSE=0.05, and cold and polar rivers have $R^2$=0.39 and RMSE=0.17. Across the entire global dataset including all climates, $R^2$=0.47 and RMSE=0.18. To ensure the validity of results obtained using the estimated dataset we verified them using the observational dataset. There are 33 reaches in the observational dataset which also contain planform data in our intermittency dataset. For these 33 reaches we observe similar trends between intermittency and *CFI* as we did using the larger estimated dataset, with a positive correlation between $I_s$ and *CFI* (fig. S1B) but no trend linking $I_w$ to *CFI* (fig. S1A). This supports our interpretation from the larger estimated dataset that planform and sediment intermittency covary.

We also observed similar trends between water intermittency and climate (N=194), with tropical and temperate regions hosting river reaches with higher $I_w$ values (fig. S2). We also note that despite most of the observational dataset being derived from measurements in North and South America, the rate of outliers (with $I > 1$) in other continents is low. These findings from the core observational water discharge dataset support our use of the estimated GQBF dataset and demonstrate the accuracy of this large estimated river discharge resource.

To estimate $Q_{s(bf)}$ we use robust sediment transport capacity equations which have been used in field settings across various settings on Earth and other planets to good effect. The results of these equations have strong agreement with field observations in the Gulf of Corinth, Greece (*13*, *14*) where sediment fluxes can be directly compared to closed basin depositional volumes. It is important to note that these relations are dependent on grain size and flow depth, which we acquired from further numerical models. The WBM model used to estimate $D_{50}$ (*5*) has as $R^2$=0.9 and the model used to estimate *H* (*6*) the measured values to within a factor of 3 for >90% of the data, so there can be strong confidence that these models are estimating grain-size and flow depth with high certainty. We note, however, that it is *H* estimates that our values of $Q_{s(bf)}$ depend on most strongly since variations in $D_{50}$ do not significantly affect the critical shear stress for sediment transport. Finally, to estimate $Q_{s(avg)}$, we used the WBMsed model, which could introduce further uncertainty, despite providing the best constraints sediment transport averages at a global scale (*4*, *5*). It has been shown to strongly predict sediment grade and transport rates observed in observational data ($R^2$=0.54 to predict average monthly sediment flux predictions) despite over- and underpredicting daily fluxes. Specifically for the bedload and suspended portion of the bedload, the observed to modelled predictions have $R^2$ values (log-log-linear) of 0.83 and 0.81, respectively (*5*). WMBsed is grounded in the BQART model for average sediment transport fluxes. When used to estimate average rates, as we do, BQART has been shown to be a powerful predictor of sediment flux in the past and can predict long-term sediment fluxes within a factor of 1.5-1.6 compared to rates acquired from erosional volumes derived from palaeo-DEMs (*15*), or depositional volumes such as in the Gulf of Corinth, Greece (*14*) where a portion of our observational $I_s$ dataset comes from. In the Gulf of Corinth, the outputs of this model can be directly compared to depositional volumes of sediment in a closed basin measured from seismic stratigraphy (*13*, *14*) which further increases our confidence in its ability to predict long-term average sediment flux rates.

The result of this uncertainty in inputs is a relatively large spread in values of water and sediment intermittency. The full distribution of intermittency factors recovered, despite its apparently broad range, still reveals that patterns observed in classified (Kruskal–Wallis H-tests) and continuous approaches that $I_s$ is significantly different depending on planform, and $I_w$ is significantly different

depending on climate, beyond uncertainty. To support these results, we conducted linear multivariate regression analyses to confirm that planform is the parameter with the strongest correlation (based on Pearson coefficient) with sediment intermittency (fig S3). This analysis supports our results that planform is the dominant determinant of $I_s$, and other catchment and channel parameters such as catchment area do not covary with channel planform, quantified by *CFI* (fig. S4).

**Extended Discussion**

Our results show that, while climate sets water intermittency, river planform primarily controls sediment transport intermittency: multi-thread rivers exhibit significantly lower sediment intermittency factors than single-thread rivers (Figure 2 in the main article). We additionally found that the relationship between *CFI* and $I_s$ is best described by a power-law trend with a quadratic formula $y=0.02x^2$, following a truncated power-law distribution (*16*) where $I_s < 1$. Halving the *CFI* (a river with twice as many threads), reduces the sediment intermittency by a factor of four. Simply, this demonstrates that intermittency is much more sensitive to changes in river planform than previously recognised. But we can also demonstrate that this reveals a mechanistic explanation for the global variability in sediment intermittency.

This finding can be mechanistically linked to scaling relations between discharge and bed shear stress (fig. S5). Consider a single-thread river that has a bankfull discharge capacity of $Q$. In this river at bankfull conditions, bed shear stress is directly proportional to bankfull flow depth, $a$. Bankfull discharge $Q$ can be described by $a$ multiplied by the bankfull river width, which is equal to the depth multiplied by a width/depth ratio, $n$, and the bankfull flow velocity, $\underline{u}$. Now consider a multi-thread river with $N_t$ threads but the same total bankfull discharge capacity. Experiments and field observations indicate that bankfull width/depth ratio ($n$) of each thread in a multi-thread river is similar to the width/depth ratio of single-thread rivers (*17*). Thus, for the same bankfull discharge, the increase in number of threads should be accommodated by a reduction in bankfull flow depth to $b$. In this multi-thread scenario, the bankfull discharge can be described by

$$Q = na^2u = nb^2uN_t.$$

Since bankfull velocities, $u$, in all large rivers are roughly constant (*18*), this can be expressed as

$$a^2 \propto b^2N_t,$$

demonstrating flow depth, and therefore sediment-transporting shear stress, varies with the number of threads in a river as a square-root term:

$$b \propto \frac{a}{\sqrt{N_t}}.$$

This explains the quadratic relationship observed between *CFI* and $I_s$, and demonstrates the sensitivity of sediment transport patterns to subtle changes in the thread count and sinuosity of rivers.

**References**


1. C. P. Galeazzi, R. P. Almeida, A. H. do Prado, Linking rivers to the rock record: Channel patterns and paleocurrent circular variance. *Geology* **49**, 1402–1407 (2021).

2. Y. Liu, M. Wortmann, L. Hawker, J. Neal, J. Yin, M. S. Santos, B. Anderson, R. Boothroyd, A. Nicholas, G. S. Smith, P. Ashworth, H. Cloke, S. Gebrechorkos, J. Leyland, B. Zhang, E. Vahidi, H. Griffith, P. Delorme, S. McLelland, D. Parsons, S. Darby, L. Slater, Global Estimation of River Bankfull Discharge Reveals Distinct Flood Recurrences Across Different Climate Zones. In Review [Preprint] (2024). https://doi.org/10.21203/rs.3.rs-5185659/v1.

3. A. T. Hayden, M. P. Lamb, B. J. McElroy, Constraining the Timespan of Fluvial Activity From the Intermittency of Sediment Transport on Earth and Mars. *Geophysical Research Letters* **48** (2021).

4. S. Cohen, A. J. Kettner, J. P. M. Syvitski, B. M. Fekete, WBMsed, a distributed global-scale riverine sediment flux model: Model description and validation. *Computers & Geosciences* **53**, 80–93 (2013).

5. S. Cohen, J. Syvitski, T. Ashley, R. Lammers, B. Fekete, H.-Y. Li, Spatial Trends and Drivers of Bedload and Suspended Sediment Fluxes in Global Rivers. *Water Resources Research* **58**, e2021WR031583 (2022).

6. S. P. D. Birch, G. Parker, P. Corlies, J. M. Soderblom, J. W. Miller, R. V. Palermo, J. M. Lora, A. D. Ashton, A. G. Hayes, J. T. Perron, Reconstructing river flows remotely on Earth, Titan, and Mars. *Proceedings of the National Academy of Sciences* **120**, e2206837120 (2023).

7. F. Engelund, E. Hansen, A monograph on sediment transport in alluvial streams. *Technical University of Denmark 0stervoldgade 10, Copenhagen K.* (1967).

8. E. Meyer-Peter, R. Müller, Formulas for Bed-Load transport. *IAHSR 2nd meeting, Stockholm, appendix 2* (1948).

9. M. Wong, G. Parker, Reanalysis and Correction of Bed-Load Relation of Meyer-Peter and Müller Using Their Own Database. *J. Hydraul. Eng.* **132**, 1159–1168 (2006).

10. G. H. Allen, T. M. Pavelsky, Global extent of rivers and streams. *Science* **361**, 585–588 (2018).

11. C. Paola, P. L. Heller, C. L. Angevine, The large-scale dynamics of grain-size variation in alluvial basins, 1: Theory. *Basin Research* **4**, 73–90 (1992).

12. H. Einstein, "The Bed-Load Function for Sediment Transportation in Open Channel Flows" (1950; https://www.semanticscholar.org/paper/The-Bed-Load-Function-for-Sediment-Transportation-Einstein/7f9d8f5699e68821d27baf02f890cd0b6a02c0ec).

13. J. S. McLeod, A. C. Whittaker, R. E. Bell, G. J. Hampson, S. E. Watkins, S. A. S. Brooke, N. Rezwan, J. Hook, J. R. Zondervan, V. Ganti, S. J. Lyster, Landscapes on the edge: River intermittency in a warming world. *Geology* **52**, 512–516 (2024).

14. S. E. Watkins, A. C. Whittaker, R. E. Bell, L. C. McNeill, R. L. Gawthorpe, S. A. S. Brooke, C. W. Nixon, Are landscapes buffered to high-frequency climate change? A comparison of sediment fluxes and depositional volumes in the Corinth Rift, central Greece, over the past 130 k.y. *GSA Bulletin* **131**, 372–388 (2019).

15. X. Yan, A. C. Whittaker, B. Gréselle, Reconciling Geologic and Paleotopographic Constraints on Source-to-Sink Sediment Fluxes: An Example From the Bartonian Pyrenees. *Basin Research* **37**, e70037 (2025).

16. S. M. Burroughs, S. F. Tebbens, Upper-truncated power law distributions. *Fractals* **09**, 209–222 (2001).

17. F. Métivier, E. Lajeunesse, O. Devauchelle, Laboratory rivers: Lacey's law, threshold theory, and channel stability. *Earth Surface Dynamics* **5**, 187–198 (2017).

18. L. B. Leopold, T. Maddock, *The Hydraulic Geometry of Stream Channels and Some Physiographic Implications* (U.S. Government Printing Office, 1953).

## Supplementary Figures

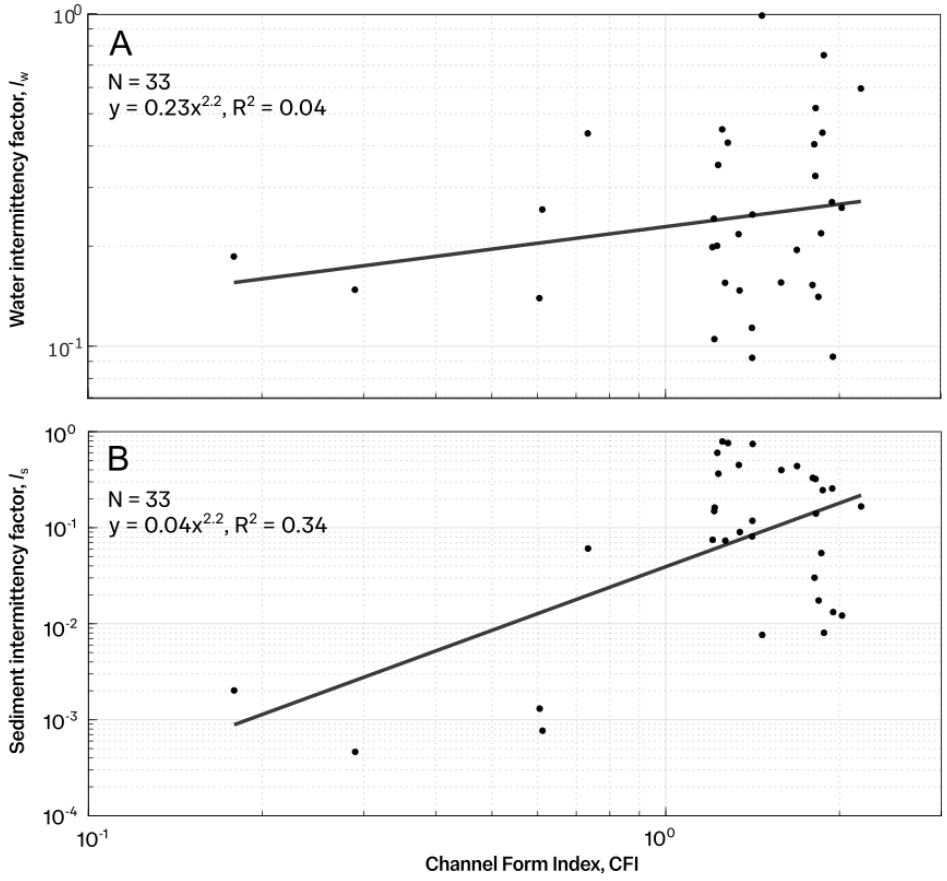


**Fig. S1.** The distribution of intermittency across planform types, using reaches within the core observational $Q_{w(bf)}$ dataset containing planform data. (A) Using observational water discharge data, $I_w$ does not correspond to *CFI*. (B) At the same reaches, $I_s$ correlates with *CFI*, with comparable trend to that observed across the whole dataset.

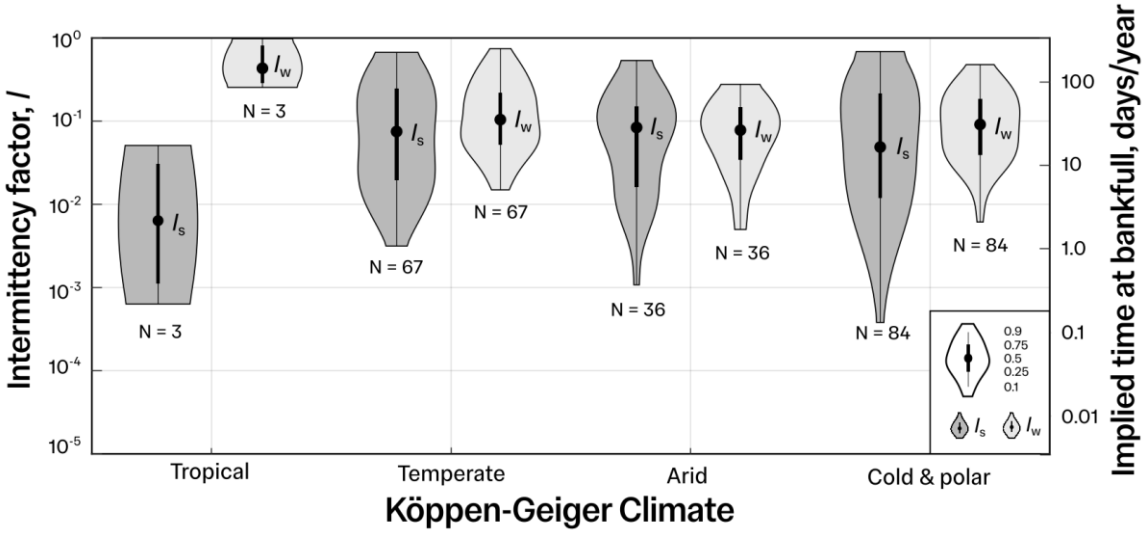


**fig. S2**. The distribution of intermittency across climate zones, using reaches within the core observational $Q_{w(bf)}$ dataset containing planform data. Using core observational dataset (N=194), we observe a similar correlation between climate and $I_w$ as with the larger estimated bankfull discharge dataset. At the same reaches, there is less of a correlation between $I_s$ and climate.

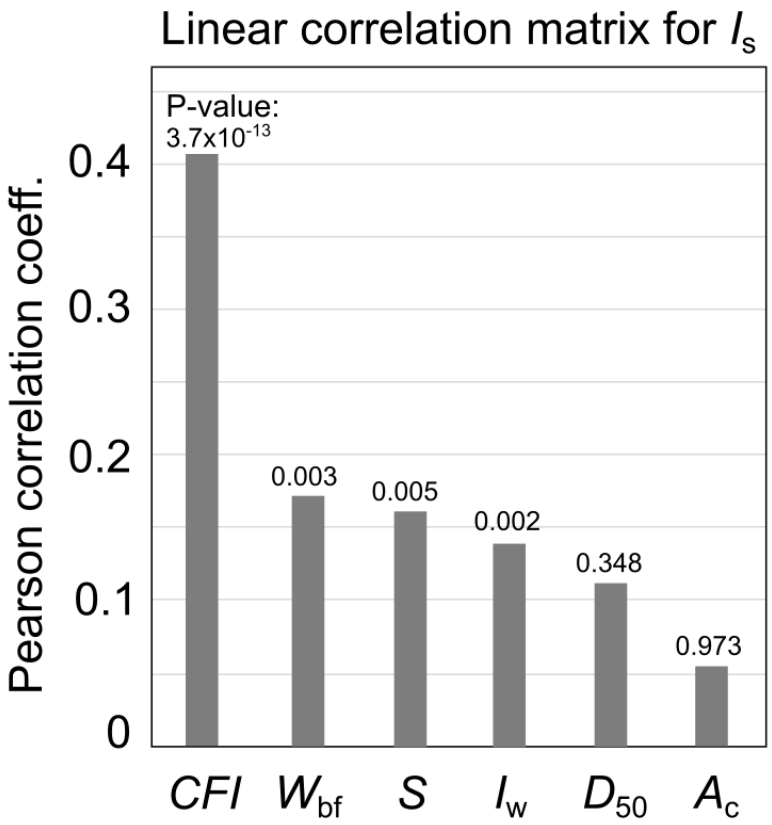


**fig. S3.** A linear correlation plot showing the different strengths of for the hydrological parameters with Pearson coefficients above 0.05, where *CFI* is the Channel Form Index, $W_{bf}$ is the bankfull river width, $S$ is the channel gradient, $I_w$ is the water intermittency factor, $D_{50}$ is the median grain-size and $A_c$ is the catchment area. Note that we show the absolute values of the Pearson coefficient: some correlations are negative. Results show that planform has the strongest correlations with sediment intermittency. *CFI* is the strongest, with a linear correlation coefficient of 0.405. Also displayed are the p-values for each correlation.

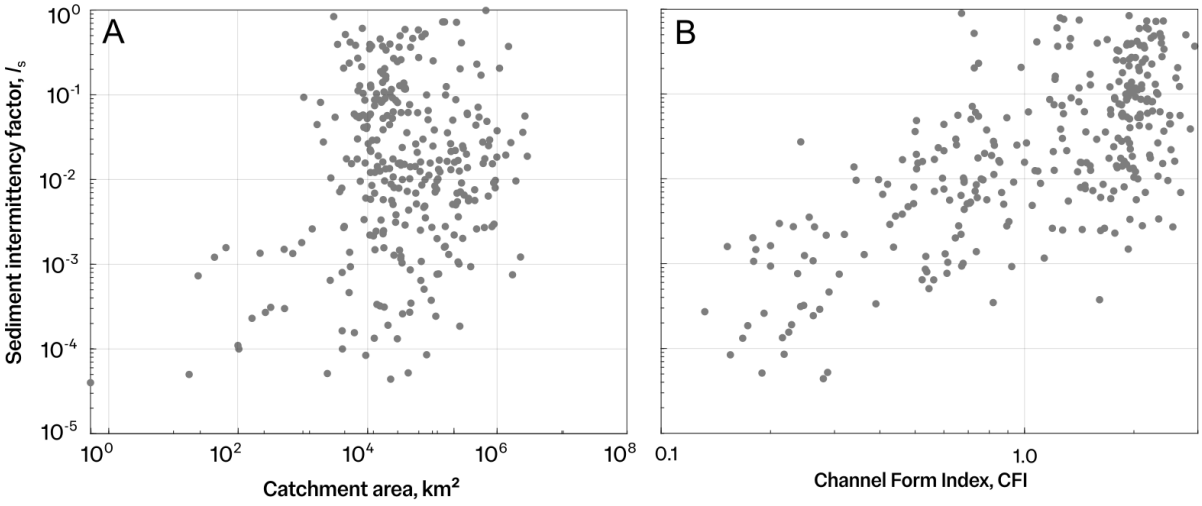


**fig. S4.** Regressions of $I_s$ with catchment area and *CFI*, the two highest and lowest correlations displayed on fig. S2.

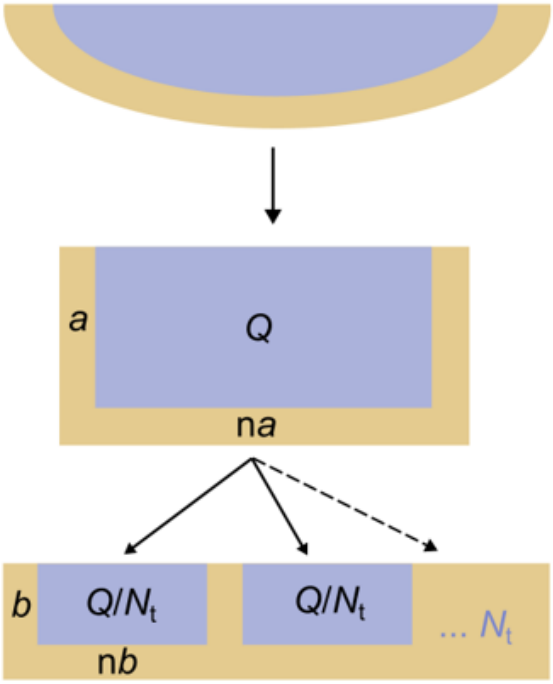


**Figure S5.** Schematic illustrating the effect of partitioning discharge between multiple river threads, where $a$ is bankfull flow depth, $Q$ is discharge, $b$ is width and $N_t$ is the number of threads.

**Supplementary data** (separate file)

Dataset containing hydrological parameters and intermittency factors used in analyses.